

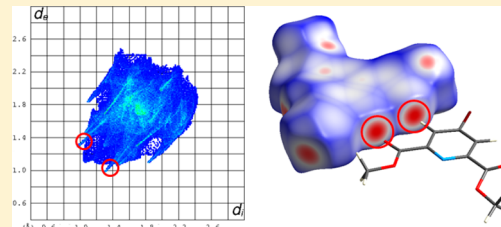
## Hirshfeld Surface Investigation of Structure-Directing Interactions within Dipicolinic Acid Derivatives

Adam D. Martin, Joshua Britton, Timothy L. Easun, Alexander J. Blake, William Lewis, and Martin Schröder\*

School of Chemistry, University of Nottingham, Nottingham NG7 2RD, U.K.

### Supporting Information

**ABSTRACT:** Six compounds based on dipicolinic acid esters have been synthesized and Hirshfeld surfaces used to investigate the structure-directing effects of functional groups in controlling their solid-state behavior. Compounds **1–4** are 4-bromo dipicolinic acid esters substituted with methyl, ethyl, propyl, and benzyl groups, respectively. The main structure-directing motif within **1–3** is a pairwise O···H interaction involving two carbonyl oxygen atoms and two aromatic H atoms. The introduction of bulky benzyl groups in **4** forces a significant change in the position of this interaction. Compounds **2** and **4** were used in Suzuki coupling reactions to prepare extended analogues **5** and **6**, respectively, and their solid-state behavior was also studied using Hirshfeld surfaces. Extension of these dipicolinic acid esters results in the complete loss of the pairwise O···H interaction in **5**, where the dominant structure-directing motifs are  $\pi$ -based interactions. However, the pairwise O···H interaction reappears for the more flexible **6**, demonstrating control of the solid-state structure of these dipicolinic acid derivatives through the choice of functional groups.



### INTRODUCTION

Controlling the solid-state behavior of molecules through the use of weak interactions is a long-standing goal of supramolecular chemistry. Two of the most popular approaches involve exploiting reversible metal coordination and hydrogen bonding.<sup>1–6</sup> The strength of hydrogen bonding interactions relative to other weak interactions means that it plays an important role in the solid-state behavior of supramolecular materials.<sup>7–11</sup> Multiple hydrogen bonding interactions, such as the pairwise O···H interaction described in this work, impart enhanced stability to supramolecular structures, such as in the multiple hydrogen bonds between complementary DNA base pairs (Figure 1, top right). This behavior can be investigated through the use of Hirshfeld surface analysis,<sup>12</sup> which allows visualization of the different types of interactions present within a crystal structure. Those pertinent to this work include H···H, C···H, N···H, O···H, halogen bonding, and  $\pi$ -based interactions. Hirshfeld surfaces are produced through the partitioning of space within a crystal where the ratio of promolecule to procrystal electron densities is equal to 0.5, resulting in continuous, nonoverlapping surfaces.<sup>13</sup> It is widely used to study polymorphs of small molecules.<sup>14</sup> However, its versatility means it can also be employed for larger supramolecular assemblies,<sup>15</sup> and Hirshfeld surface analysis is particularly useful in studying how different functionalities can affect crystal packing behavior.<sup>16</sup> In this latter work, it was found that for *para*-substituted phenols, changing the functionality from *tert*-butyl to benzyl to nitro results in the dominant interaction in the structures changing from H···H to C···H and O···H interactions, respectively. This information is not readily apparent solely from the crystal structure and explains the

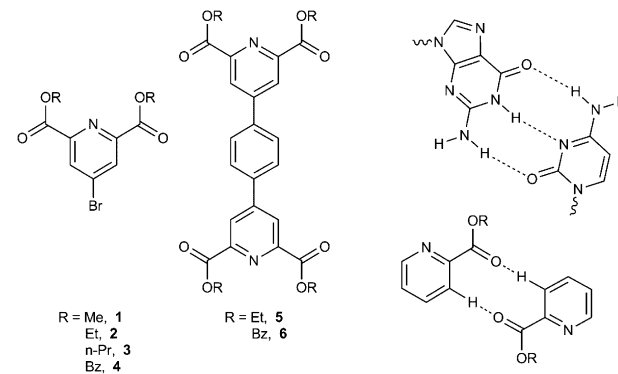


**Figure 1.** Dipicolinic acid derivatives synthesized in this work (left, center), triple interaction between DNA bases G and C (top right), and the pairwise O···H interaction observed in **1**, **2**, **3**, **4**, and **6** (bottom right).

significant change in packing behavior observed for these compounds.

Dipicolinic acid and its derivatives can form a variety of supramolecular structures with lanthanides, including triple helices and polymeric networks,<sup>17,18</sup> with the luminescence of the lanthanides often enhanced via strong, tridentate coordination to the dipicolinic acid site.<sup>19</sup> Coordination polymers with copper, cobalt, and zinc have been reported,<sup>20–24</sup> as has a La(III)-based metal–organic frame-

**Received:** November 20, 2014

**Revised:** January 18, 2015

**Published:** March 20, 2015

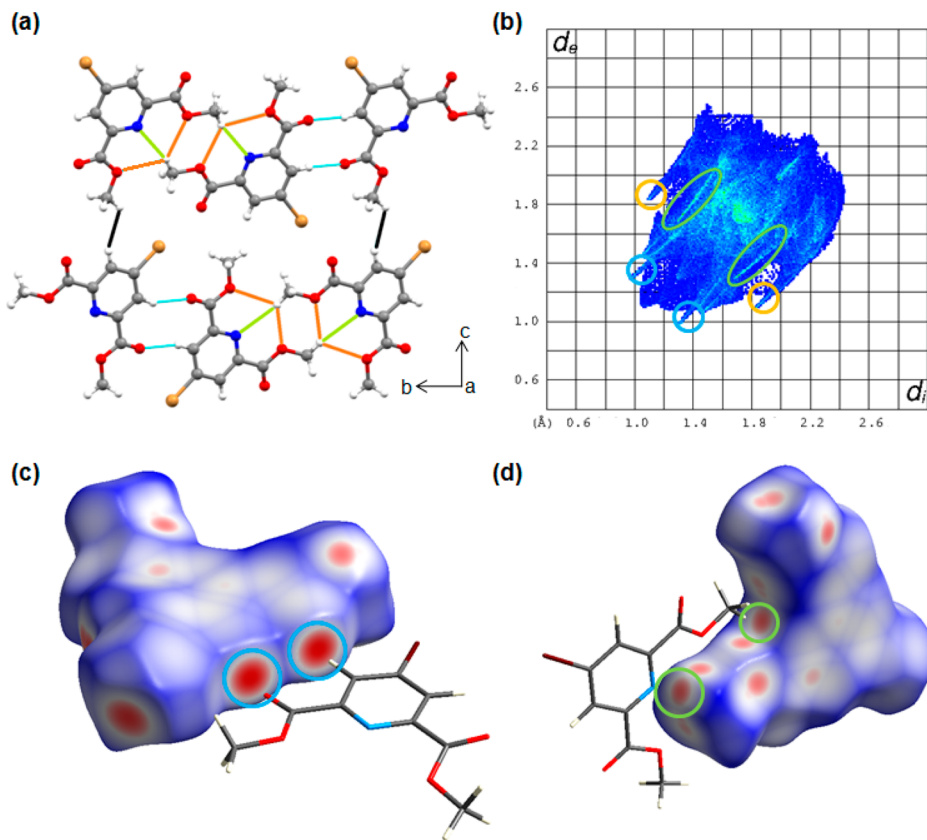


**Figure 2.** (a) Packing diagram with short contacts highlighted: N···H (green), pairwise O···H (blue), other O···H (orange), and H···H (black). (b) Fingerprint plot with characteristic interactions circled: N···H (green), O···H (blue), and Br···H (yellow). (c)  $d_{norm}$  surfaces displaying the pairwise O···H interaction (blue) and (d) N···H interaction (green circles) for **1**.

work,<sup>25</sup> which illustrates the versatility of these dipicolinic acids in the formation of supramolecular structures. The major feature in all of these examples is tridentate coordination via the carboxylic acids situated at the 2- and 6-positions of the pyridyl ring, allowing charge delocalization to stabilize the structures. In order to allow other structure-directing interactions such as hydrogen bonding to be investigated, the charge delocalization can be blocked and steric interactions enhanced by the introduction of ester groups, thus suppressing this tridentate binding mode.

Herein we report the synthesis of four 4-bromo dipicolinic acid esters, **1–4**, systematically varying the ester substituent in order to assess the effect of functional groups on the solid-state behavior of these systems. Two of these esters, **2** and **4**, are extended through a coupling reaction to give conjugated systems **5** and **6**, respectively, in which the flexibility of the ester group plays an important role in determining the nature of interactions observed within the crystal structure. The solid-state structures of compounds **1–6** were studied through the use of Hirshfeld surface analysis, which has allowed visualization of the proportion and nature of the interactions present in the structures, some of which are not readily apparent through examination of the crystal structure alone. The importance of the double O···H interaction (Figure 1, bottom right) as a structure-directing motif is highlighted, and the impact on this interaction of varying the ester substituents is discussed.

## RESULTS AND DISCUSSION

4-Bromopyridine-2,6-dicarboxylic acid was synthesized according to a literature procedure<sup>26</sup> and **1–4** obtained via reaction with the corresponding alcohols. Compounds **5** and **6** were synthesized via Suzuki coupling procedure using **2** and **4**, respectively.<sup>27</sup> Single crystals of **1–4** suitable for X-ray diffraction studies were obtained by recrystallization in diisopropyl ether, and crystals of **5** and **6** were grown by recrystallization of the compounds from CH<sub>2</sub>Cl<sub>2</sub> and MeOH.

Compound **1** crystallizes in the triclinic space group  $\overline{P} \bar{1}$  with two molecules in the asymmetric unit. These molecules stack in an eclipsed manner down the *a* axis with no  $\pi-\pi$  stacking interactions evident. There is a pairwise O···H interaction of 2.378(4) Å,  $\angle C=O \cdots H = 154^\circ$ , between the carbonyl oxygen from one molecule and an aromatic proton from an adjacent molecule (highlighted in cyan in Figure 2a). This feature is also observed in compounds **2** and **3** and appears to be the main structure-directing interaction within the crystal structure. A short contact [2.30(3) Å] is also observed wherein one of the methyl protons interacts with the pyridyl nitrogen and is highlighted in green in Figure 2a. Interestingly, this is the only bromopyridyl compound where the pyridyl nitrogen participates in intermolecular interactions, a feature discussed further below.

When Hirshfeld surfaces were proposed as an effective way to discern intermolecular interactions in the solid state, the first properties to be mapped on this surface were  $d_e$  and  $d_i$ , the distances of an atom external or internal to the generated Hirshfeld surface. Combining these two values results in a ( $d_i$ ,  $d_e$ ) pair, and binning these into intervals of 0.01 Å (essentially a

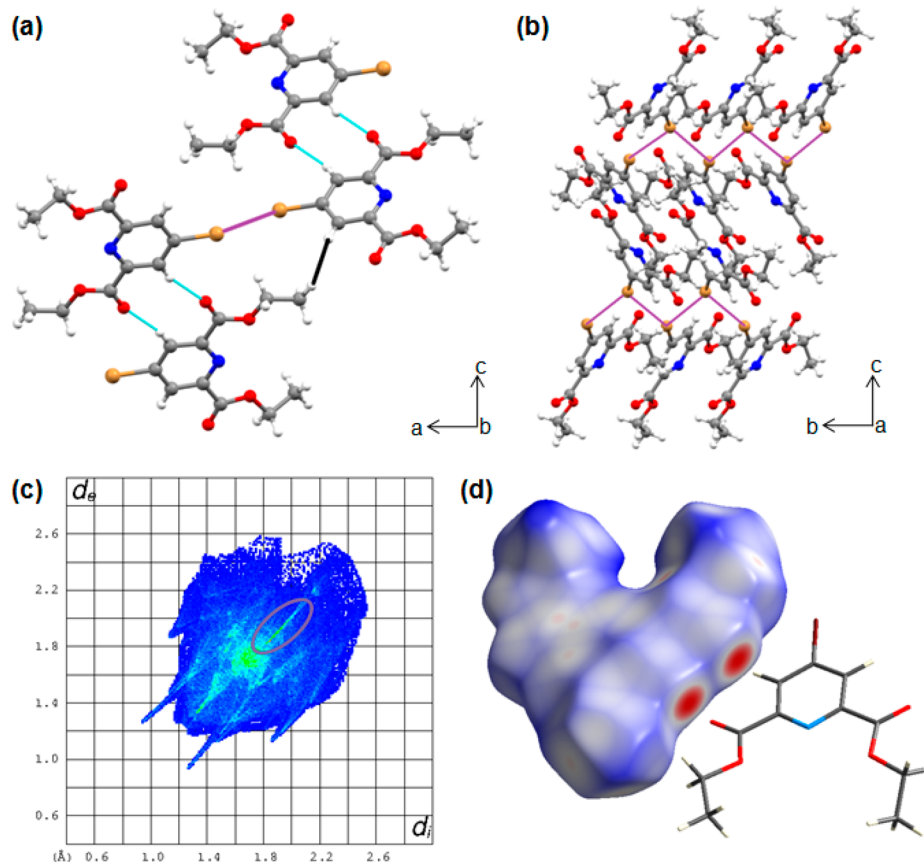


**Figure 3.** (a) Packing diagram down the *b* axis showing short O···H (blue) and Br···Br (purple) contacts, (b) packing down the *a* axis, (c) fingerprint plot with Br···Br interactions highlighted (purple), and (d)  $d_{\text{norm}}$  surface for 2.

pixel on the Hirshfeld surface) results in the generation of a fingerprint plot, where the different colors on the fingerprint plot represent the frequency of occurrence of the interaction, increasing from blue to green to red. Taking these ( $d_i$ ,  $d_e$ ) pairs and normalizing them with respect to the van der Waals radii of their corresponding atoms results in the  $d_{\text{norm}}$  surface, with contacts shorter than the sum of the van der Waals radii of the two atoms resulting in a negative value and being highlighted on the  $d_{\text{norm}}$  surface in red. Contacts close in length to the van der Waals limit are colored white, and blue represents longer contacts.<sup>28</sup>

The Hirshfeld surface analysis for **1** shows the lowest proportion of H···H interactions for all of the structures studied, making up only 25.9% of the surface. This is to be expected since **1** has only methyl esters with proportionally fewer hydrogen atoms than compounds **2–6**. Only one short H···H contact is present due to a hydrogen from a methyl group interacting with an adjacent aromatic hydrogen [2.330(6) Å,  $\angle = 112^\circ$ , highlighted in black in Figure 2a]. O···H and H···O interactions combined, represented as spikes circled by blue in Figure 3b, comprise 26.0% of the surface. One close contact is the pairwise interaction also seen in compounds **2**, **3**, and **6**, whereby a carbonyl oxygen interacts with an aromatic proton, highlighted in blue in Figure 2c. The other close contact results from an OCH<sub>3</sub> oxygen oriented toward a hydrogen from a neighboring methyl group [2.61(4) Å,  $\angle = 119^\circ$ , highlighted in orange in Figure 2a]. Br···H interactions, circled in yellow in Figure 2b, comprise 10.4% of the Hirshfeld surface but are all moderate to long contacts (3.0–4.4 Å). A short Br···O contact [2.98(7) Å] is also present

for one of the molecules in the asymmetric unit, where the Br atom is directed toward the carbonyl oxygen that does not participate in the O···H double interaction. This interaction comprises 6.1% of the Hirshfeld surface for this molecule. N···H contacts, highlighted in green in Figure 2a, only make up 1.4% of the Hirshfeld surface but are significant because it is only in **1** and **6** that N···H contacts are observed at all. When larger ester groups are employed, the nitrogen is sterically blocked and cannot participate in intermolecular interactions. In the case of **1**, a neighboring methyl proton is directed toward the pyridyl nitrogen, resulting in a short contact [2.60(3) Å],  $\angle = 123^\circ$ , circled in green on the  $d_{\text{norm}}$  surface in Figure 2d). This interaction is the other major structure-directing feature seen in this crystal structure and is the reason that **1** packs in a significantly different manner to **2** or **3**. Hirshfeld surface analysis of the other molecule in the asymmetric unit reveals that aside from the aforementioned Br···O contact, the interactions present for this molecule only vary in their proportion (<0.2%) and not in their nature.

Compound **2** crystallizes in the monoclinic space group  $P2_1/n$  with one molecule in the asymmetric unit. The molecules pack in a herringbone arrangement along the *a* axis, and stack in an eclipsed manner down the *b* axis (Figure 3a). A zigzag chain of Br atoms is visible when viewed down the *a* axis (Figure 3b) and involves a short Br···Br contact of 3.639(7) Å ( $\angle \text{Br} \cdots \text{Br} \cdots \text{Br} = 73.2^\circ$ , highlighted in Figure 3a in purple). The pairwise O···H interactions are highlighted in blue in Figure 3a [2.350(5) Å,  $\angle (\text{O} \cdots \text{H}) = 165.9^\circ$ ] and constitute the same motif as that observed in **1**, **3**, and **6**.

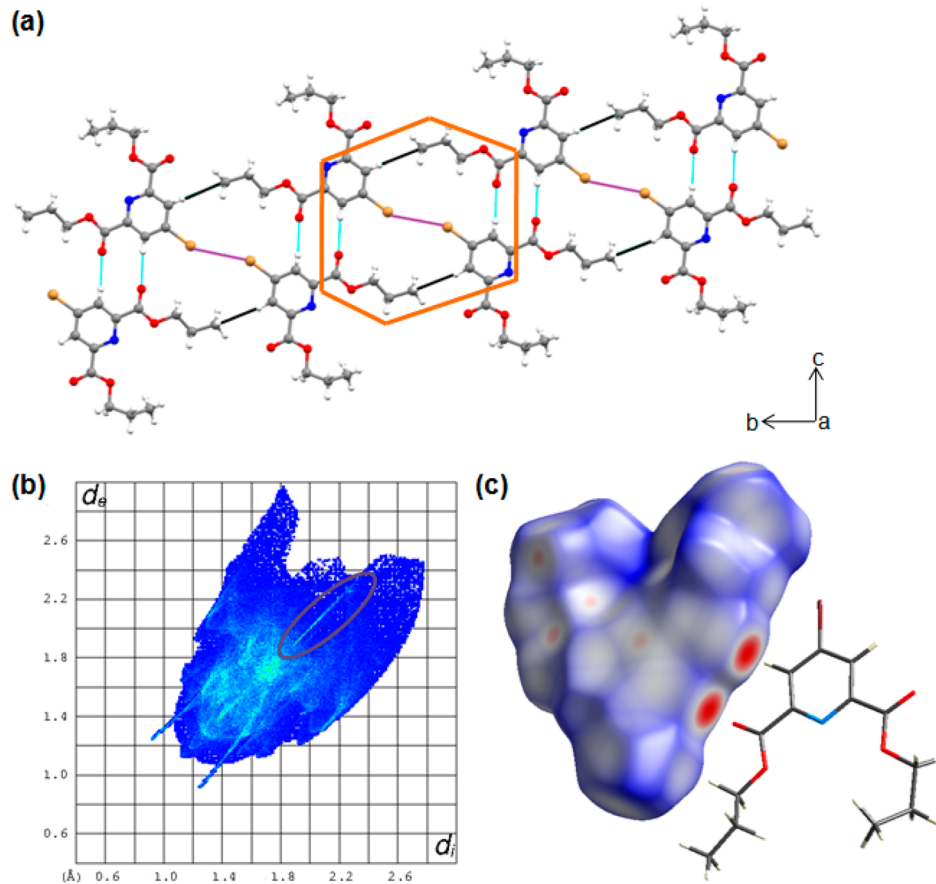


**Figure 4.** (a) Packing diagram highlighting a circuit of close contacts (orange), short O··H contacts (blue), and H··H (black) contacts, (b) fingerprint plot with Br··Br interactions circled (purple) and (c)  $d_{\text{norm}}$  surface showing the pairwise O··H interaction for 3.

Hirshfeld surface analysis of **2** shows that H··H contacts make up 37.7% of the surface, with one short contact present between an aromatic proton and an ester proton from a nearby molecule ( $2.797(4)$  Å,  $\angle = 109.4^\circ$ , highlighted in black in Figure 3a). The proportion of H··H interactions has increased from **1** since the longer alkyl chain affords a higher proportion of hydrogen atoms in the structure. O··H and H··O interactions comprise 21.8% of the surface, with one close contact arising from the interaction of an oxygen center from an  $\text{OCH}_2\text{CH}_3$  moiety with a neighboring methylene proton. This interaction occurs down the *b* axis and is perpendicular to the pairwise O··H interaction described above, unlike the related interaction observed for **1** in which the ester  $\text{OCH}_3$  oxygen interacts with a hydrogen on an adjacent methyl group, in the same plane as the pairwise O··H interaction.

The zigzag chain of Br atoms seen in the crystal structure of **2** is displayed on the fingerprint plot as a bright streak circled in purple in Figure 3c, representing only 2.9% of the surface. This low percentage only relates to a proportion of interactions (given that there is only one Br in the structure, this number will generally be low) and does not reflect the strength and structure-directing effect that such an interaction has on the solid-state behavior of the molecule.

Previous studies on halogen··halogen interactions have shown that generally one of two different types of interaction will occur.<sup>29</sup> A type-I interaction is when  $\theta_1 \approx \theta_2$  (where  $\theta_1$  is the angle C–Br<sub>1</sub>··Br<sub>2</sub> and  $\theta_2$  is the angle C–Br<sub>2</sub>··Br<sub>1</sub>) and a type-II is characterized by  $\theta_1 \approx 90^\circ$  and  $\theta_2 \approx 180^\circ$ .<sup>30</sup> In the case of **2**, a type-I interaction with  $\theta_1 \approx \theta_2 \approx 133^\circ$  exists as a

consequence of close packing that serves to minimize repulsion between adjacent Br atoms.<sup>31</sup> The two ethyl ester moieties of **2** do not allow the pyridyl nitrogen to participate in any intermolecular interactions, a key difference from **1**, resulting in a different packing motif that forces the Br atoms to be oriented toward each other and producing the alternating chain of Br atoms. Although the more flexible ethyl esters force a deviation from the formation of planar sheets observed in **1**, the pairwise O··H interaction remains and is in fact shorter than that observed in **1**.

Compound **3** crystallizes in the monoclinic space group  $P2_1/n$  with one molecule present in the symmetric unit. Disorder of one of the propyl groups over two positions was modeled prior to Hirshfeld surface analysis. A herringbone arrangement down the *b* axis similar to compound **2** is observed, but no corresponding zigzag arrangement of Br atoms is seen; instead, the Br atoms are involved in an end-on interaction with each other, similar to that observed in **4** below. Again, the pairwise O··H interaction [2.311(3) Å] and eclipsed stacking down the *a* axis are evident. Figure 4a shows that when viewed across the *bc* plane there is a hexagonal shaped circuit of close contacts (outlined in orange) in the plane involving the pairwise O··H interaction (highlighted in blue) and a short H··H contact (highlighted in black). It is noteworthy that as the length of the alkyl substituent has increased, this pairwise O··H interaction distance has shortened from 2.378 to 2.350 to 2.311 Å for **1**, **2**, and **3**, respectively. This is consistent with the larger alkyl substituents affording greater flexibility within the

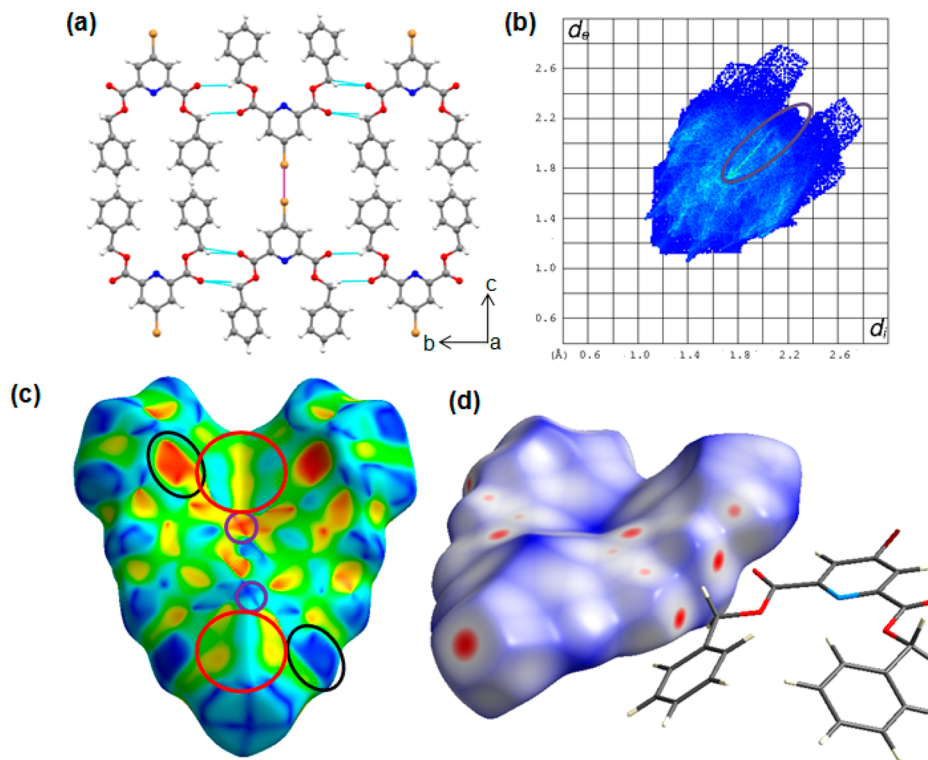


**Figure 5.** (a) Packing diagram with O...H (blue) and Br...Br (purple) contacts highlighted, (b) fingerprint plot with Br...Br region circled (purple), (c) shape index with areas of complementarity identified (paired circles), and (d)  $d_{\text{norm}}$  surface showing pairwise O...H interactions for 4.

structure, resulting in more efficient packing and a shorter pairwise O...H interaction distance.

Hirshfeld surface analysis of 3 shows unsurprisingly that it contains the highest proportion of H...H interactions for compounds 1–4 (44.7%), a consequence of the higher proportion of hydrogen atoms in the structure afforded by the longer alkyl esters. Of the atoms present in 3, 45.7% are hydrogens in contrast to 41.3% and 34.8% for 2 and 1, respectively, so it is no surprise that H...H interactions dominate the Hirshfeld surface. Short contacts arise both from interactions between ester protons and from an aromatic proton directed toward an ester proton in a manner analogous to that observed in 2, which is to be expected given their similar packing arrangements. Of the compounds 1–4, compound 3 contains the highest proportion of long (4.0–5.5 Å) H...H contacts due to the disordered nature of one propyl chain resulting in more space between adjacent Br atoms than for 1 or 2 (see Figure 4a). This results in the appearance of asymmetric “wings” at the top of the fingerprint plot (Figure 4b) and is reflected in the lower crystal density (1.547 g/cm<sup>3</sup> for 3 compared with 1.844 and 1.637 g/cm<sup>3</sup> for 1 and 2, respectively). O...H and H...O interactions only comprise 17.2% of the surface and, again owing to the similarity of the structures, their nature is very similar to that observed in 2, with one short contact due to the pairwise O...H interaction, Figure 4c. Where 3 differs from 1 and 2 is that the other carbonyl oxygen (i.e., the one not participating in the pairwise interaction) is involved in a short contact with a methylene proton from a neighboring ester group, whereas for 1 and 2 this carbonyl is not involved in any short contacts. Br...Br interactions are also present in 3 as in 2, but the distance between adjacent Br atoms is larger [3.792(6) in 3 vs 3.639(7) Å in 2], resulting in a shift in the position of the Br...Br streak in the fingerprint plot, Figure 4b. It should be noted that as in

2, the Br...Br interaction is a type-I interaction, but in this case,  $\theta_1 \approx \theta_2 \approx 156^\circ$ , compared to 133° for 2.

Given the solid-state packing observed in 1–3, it was argued that a bulkier ester substituent would result in a completely different packing mode, which could allow us to investigate other possible interactions between dipicolinic cores. With this in mind, we synthesized the analogous benzyl ester 4 to examine whether the dominant structure-directing feature would change from the pairwise O...H interaction observed in 1–3. Compound 4 crystallizes in the triclinic space group  $P\bar{1}$  with one molecule in the asymmetric unit. The benzyl groups are tilted at 43° and 41° in relation to the pyridyl ring, and the molecules pack in an alternating “up–down” arrangement down the *a* axis (Figure 5a). There is a form of pairwise O...H interaction present, but this interaction is markedly different to that observed in 1–3 and 6. In 4, this short contact occurs between CH<sub>2</sub> protons from the benzyl ester and a carbonyl oxygen, highlighted in blue in Figure 5a. It does not involve an aromatic pyridyl proton, unlike the pairwise interactions observed in 1–3. This results in an increase in the O...H interaction distance [2.625(5) Å for 4 vs ca. 2.3 Å for 1–3]. The change in this interaction can be attributed to the bulkier nature of the ester substituent since a similar packing arrangement and associated pairwise O...H interaction to those observed for 1–3 would result in large void spaces throughout the molecule. A short end-on Br...Br contact is also observed in the structure, highlighted by the purple interaction in Figure 5a. This contact is a type-I interaction ( $\theta_1 \approx \theta_2 \approx 143^\circ$ ) similar to that observed in 3, but it is much shorter in this instance [3.489(7) Å in 4 vs 3.792(6) Å in 3], as can be seen in Figure 5(b, circled).

Shape index is a feature of Hirshfeld surface analysis that allows for identification of complementarity between molecules in the crystal packing structure. Features on the shape index

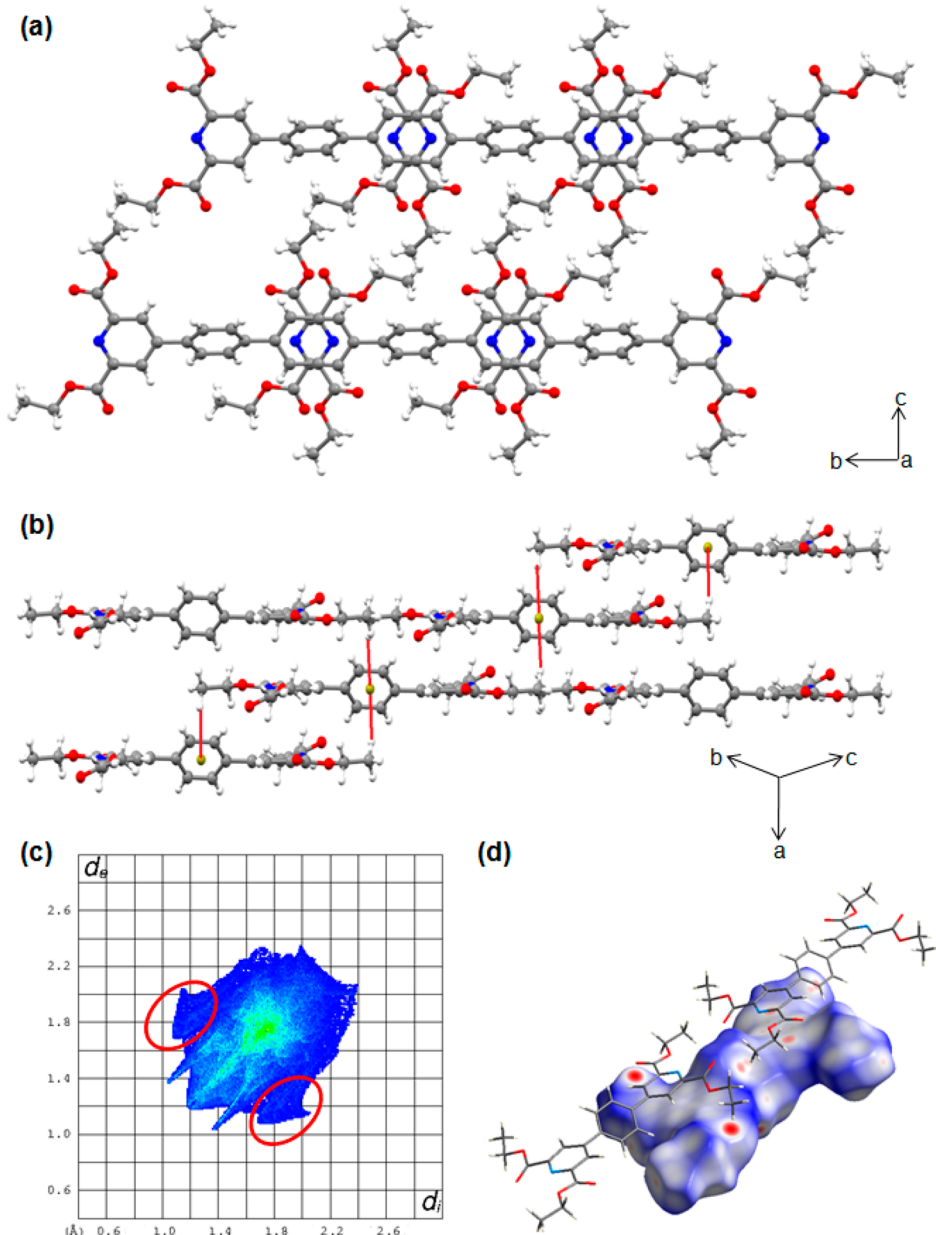


**Figure 6.** (a) Packing diagram, (b) packing diagram illustrating  $\text{CH}\cdots\pi$  contacts (red), (c) fingerprint plot showing  $\text{CH}\cdots\pi$  interactions (red circles), and (d)  $d_{\text{norm}}$  surface for **5**.

surface that have an identical pattern but opposite colors indicate areas of intermolecular complementarity. These areas are clearly visible in Figure 5c and are circled in paired colors. From the shape index surface it can be seen that the Br atom from one molecule of **4** sits between two benzyl moieties that are curved toward it, circled in red in Figure 5c. The crosses circled in purple correspond to the nitrogen of the pyridyl ring sitting between the two methylene groups from the benzyl moieties, and the matching black circles depict an area of complementarity where an aromatic proton from the pyridyl ring is positioned over a benzyl group. This complementarity helps to understand the alternating up-down packing arrangement along the *a* axis.

Hirshfeld surface analysis of **4** shows an increased amount of C...H and H...C interactions compared to structures **1–3**, accounting for 27.3% of the surface, in accordance with the replacement of alkyl esters with a benzyl group. The increased

proportion of C...H interactions does not manifest itself as short contacts or  $\text{CH}\cdots\pi$  interactions within the structure, instead appearing as medium or longer range contacts (3.2–4.4 Å). As would be expected, a smaller proportion of O...H contacts are observed, making up only 12.7% of the surface. The only short contact is due to the pairwise interaction described above, which occurs for *both* of the carbonyl oxygens, Figure 5d. This is significantly different to that seen in **1–3**, where the pairwise interaction is only present for *one* of the carbonyl oxygens. As a result, **4** displays a chain of pairwise O...H interactions down the *b* axis that is not observed for **1–3**. H...H interactions comprise 33.8% of the surface, and a short contact exists between a methylene proton and the neighboring hydrogen from a benzyl moiety. Although only 1% of the surface is assigned to Br...Br interactions, a bright streak is still visible at the top right of the fingerprint plot (as for **2** and **3**), circled in purple in Figure 5b. Like the Br...Br interactions

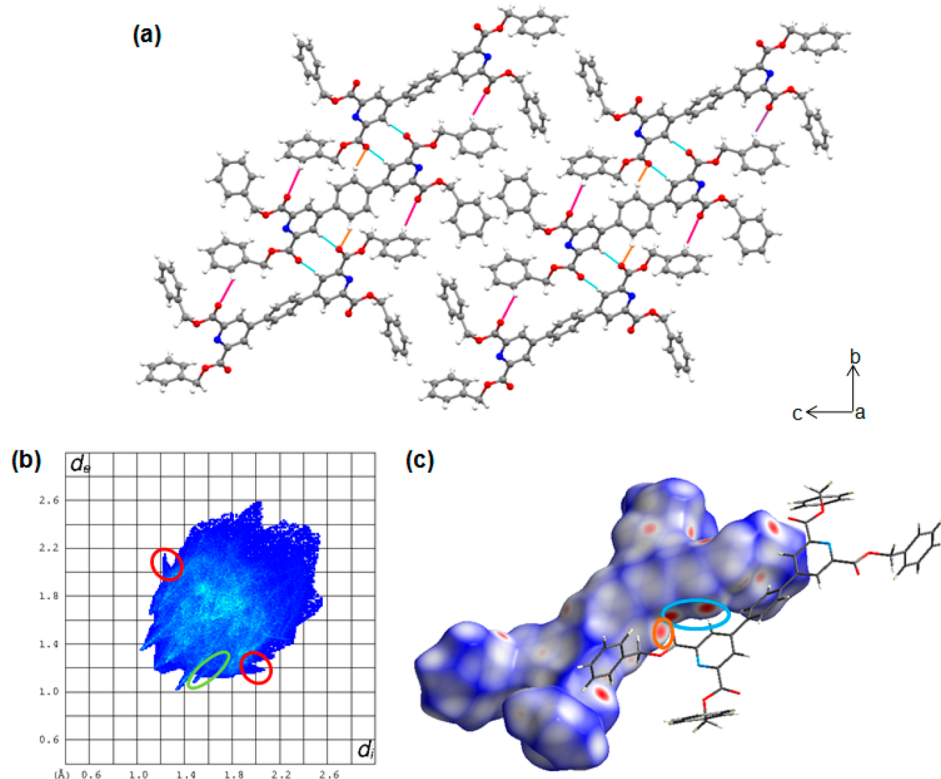


**Figure 7.** (a) Packing diagram showing the return of the pairwise O···H interaction (blue) and other O···H single interactions (orange and pink), (b) fingerprint plot displaying CH··· $\pi$  (red) and N···H (green) interactions, and (c)  $d_{\text{norm}}$  surface with unique pairwise interaction (see text) highlighted (blue and orange) for **6**.

observed in **2**, this is a type-I interaction, minimizing electrostatic repulsion between Br atoms, with  $\theta_1 = \theta_2 = 142.6^\circ$ . The primary difference from **2** is that this interaction occurs as indiscrete Br···Br pairs and not within a continuous chain throughout the structure.

In addition to systematic alteration of the ester groups, these dipicolinic acids were extended synthetically at the position *para* to the pyridyl nitrogen and the behavior of the subsequent derivatives investigated. Extension of the compounds was achieved through a Suzuki coupling employing the 4-bromo dipicolinic acid ester of choice and 1,4-benzene diboronic acid. In this way we utilized **2** and **4** to produce compounds **5** (ethyl esters) and **6** (benzyl esters), respectively. Clearly this strategy removes all possibility of halogen bonding and it was postulated that the addition of more aryl rings to the compound would encourage  $\pi$ - $\pi$  and CH··· $\pi$  interactions. The effect of these interactions in altering the structure-directing pairwise O···H interactions observed in **1–4** is of particular interest and has implications for the design and control of hydrogen-bonded supramolecular structures.

Compound **5** crystallizes in the triclinic space group  $P\bar{1}$  with half a molecule in the asymmetric unit. The molecules are staggered along the *a* axis, with the nitrogen from one pyridyl group directly above the center of the pyridyl ring below it (and vice versa) essentially in ABAB layers (Figure 6a). This  $\pi$ -based interaction plays a critical role in the solid-state structure of **5**. The central phenyl ring is tilted at  $44^\circ$  with respect to the pyridyl rings and results in a chain of CH··· $\pi$  interactions through the ester and the central phenyl rings, highlighted in red in Figure 6c. This is the first instance of CH··· $\pi$  interactions observed for the dipicolinic acid esters reported herein and suggests a significant change in the structure-directing

interactions for **5**. Further evidence for this change is provided by the *complete absence* of the pairwise O···H interaction that is observed in compounds **1–4**, with this previously dominant feature now replaced by CH··· $\pi$  and  $\pi$ -stacking interactions. In this way, by extending the dipicolinic acid **2** to form **5** we have completely removed the pairwise O···H interaction and demonstrated control over the solid-state structure of the resulting material. The absence of any pairwise O···H interaction is unique to **5** in this study, and we assign this to a combination of the structural demands of the phenyl spacer, both in terms of the geometric restrictions it imposes on the pyridyl rings and the  $\pi$ -based interactions it undergoes, and the use of the relatively small ethyl ester. Further evidence for the effect of the latter is seen in the structure of **6** and described further below.

H···H interactions make up the majority of the Hirshfeld surface for **5**, which is consistent with the high proportion of hydrogen atoms in the structure. Although O···H and H···O interactions contribute 23.4% to the surface, it is important to note that the O···H pairwise interaction observed in **1–4** is no longer present in this structure. Instead, a short contact arises where the hydrogen from one methyl group interacts with a carbonyl oxygen, clearly visible on the  $d_{\text{norm}}$  surface in Figure 6d. A hydrogen from the other methyl group is oriented toward the central phenyl ring, resulting in characteristic CH··· $\pi$  interactions being clearly visible in Figure 6b and on the fingerprint plot as “wings” that are circled in red in Figure 6c. Although the N···C interaction observed in the structure comprises only a small fraction of the Hirshfeld surface (1.4%), it is not observed in **1–4**, and as such clearly plays a central role in the behavior of **5** in the solid-state. As noted previously in the text, the percentage of the Hirshfeld surface does not

Table 1. Selected Interactions ( $\text{\AA}$ ) and Densities ( $\text{g cm}^{-3}$ ) for Structures 1–6

interaction	1	2	3	4	5	6
O···H pairwise	2.378(4)	2.350(5)	2.311(3)	2.625(5)	no	2.505(4)
O···H other carbonyl	no	2.701(4)	2.678(3)	N/A	2.512(4), 2.653(6)	2.532(4), 2.591(4)
ester O···H	2.61(4), 2.71(3)	no	no	no	no	no
N···H	2.60(3)	no	no	no	no	2.686(5)
Br···Br	no	3.639(7)	3.792(6)	3.489(7)		
$\pi\cdots\pi$ (centroid)	no	no	no	no	3.47(8)	no
CH··· $\pi$ (centroid)	no	no	no	no	2.75(7)	3.27(8)
density	1.84	1.64	1.55	1.56	1.35	1.39

necessarily reflect the strength and structure-directing properties of the interaction.

The related observations that increasing steric bulk in compounds 1–3 decreased the pairwise O···H interaction distance and that in benzyl ester-containing 4, both carbonyl groups were accessible for the pairwise interaction rather than just one prompted us to consider whether a bulkier ester functionality than that of 5 could reinstate the pairwise O···H interaction. Therefore, compound 4 was extended via a Suzuki coupling identical to that described earlier, yielding the benzyl ester-substituted 6.

Compound 6 crystallizes in the triclinic space group  $P\bar{1}$  with two half-molecules in the asymmetric unit. The central phenyl rings are tilted at  $26^\circ$  and  $36^\circ$  with respect to the pyridyl rings for the two half-molecules, which is less than for those in 5. Because of this decreased tilt angle and the benzyl ester moieties being bulkier than the ethyl groups in 5, the central phenyl group is inaccessible for CH··· $\pi$  interactions. The benzyl ester moieties are twisted with respect to the pyridyl ring at angles of  $90$  and  $119^\circ$  for one of the molecules in the asymmetric unit, and  $90$  and  $137^\circ$  for the other molecule. The compound packs in a herringbone arrangement along both the  $a$  and  $b$  axes, and the N···C interactions that are observed in 5 are no longer present in 6 due to the bulky nature of the benzyl esters.

Notably, we have re-established the pairwise O···H interaction in 6, and as for compounds 1–3, this is based upon the interaction of a carbonyl oxygen with an aromatic proton. In this instance, however, the contact distance is longer than for 1–3 [2.505(4)  $\text{\AA}$  compared to ca. 2.3  $\text{\AA}$ ]. Also, consistent with the interaction seen for 1–3, only one of the carbonyl groups at each end of the molecule engages in the pairwise O···H interaction, and the oxygen interacts with an aromatic proton, unlike in 4. In fact, despite the same ester functionality, the pairwise O···H interaction in 6 has more in common with those observed in 1–3 than in 4. This suggests that the most favored form of the pairwise O···H interaction is between a carbonyl oxygen and an aromatic proton, and the increased bulk and flexibility of 6 compared with 4 allows this structure-directing interaction to be achieved.

Similar to 5, H···H interactions comprise the majority of the Hirshfeld surface for 6, making up 40–42% for each molecule in the asymmetric unit. This is the only structure where no short H···H contact exists, with 1–5 displaying at least one such interaction. O···H-based interactions are responsible for 16–19% of the surface in 6, with one short contact arising from the pairwise O···H interaction described previously. This interaction can clearly be seen on the  $d_{\text{norm}}$  surface (circled in blue, Figure 7c). Two other O···H close contacts exist on the structure, one involving a carbonyl oxygen and a hydrogen from the central phenyl ring (circled in orange), and one between

the other carbonyl oxygen and a benzyl hydrogen, highlighted in pink in Figure 7a. The first of these O···H close contacts involving the central phenyl ring differentiates the pairwise O···H interaction in 6 from those observed in 1–3 since one of the carbonyl oxygens of the pairwise interaction interacts with *two* aromatic protons (the second proton is circled in orange in Figure 7c) rather than simply one. Furthermore, as described above, these O···H interactions are significantly different from those observed in 4, further pointing to the structure-directing role of the central phenyl spacer in the solid-state behavior of these molecules.

The smaller proportion of H···H and O···H interactions results in a larger proportion of C···H interactions, which comprise approximately 18% of the surface of 6. One of the half molecules in the asymmetric unit contains a CH··· $\pi$  short contact, whereby a hydrogen from the central phenyl ring is directed toward a benzyl ester group. This is circled in red on the fingerprint plot in Figure 7b. This is notably different to the type of CH··· $\pi$  interaction observed in 5, where the central phenyl spacer acts as the source of  $\pi$  electrons as opposed to the source of a hydrogen in 6. The same half-molecule contains a close contact between a pyridyl nitrogen and a hydrogen from an adjacent benzyl ester moiety, which can be seen on the fingerprint plot as the spike circled in green in Figure 7b. This intermolecular contact arises due to the flexible nature of the ester, as the benzyl group of one molecule is able to rotate around the  $\text{CH}_2$  bond and position itself between two benzyl ester functionalities present in the next molecule. Other than the methyl–H interaction with the pyridyl nitrogen in 1, this is the only other compound in the series to display a N···H interaction. This interaction does not comprise a large portion of the Hirshfeld surface, but it does illustrate how the flexibility of the ester moiety is able to influence the efficiency of packing within 6, further supported by the increase in density of 6 over that of 5 (1.39 vs 1.35  $\text{g/cm}^3$  respectively).

## CONCLUSION

We have synthesized four 4-bromo dipicolinic acid derivatives 1–4 in order to assess the effect of different ester functionalities on the behavior of these molecules in the solid-state, with the key interactions summarized in Table 1. For compounds 1–3 the dominant structure-directing motif is a pairwise O···H interaction between a pair of carbonyl oxygens and aromatic protons, with the length of this pairwise interaction decreasing for longer alkyl ester chain lengths. The carbonyl oxygen not involved in the pairwise interaction only participates in a short contact in 3, whereas interactions incorporating the ester oxygens are only seen in 1, most likely due to the lack of steric hindrance associated with the methyl group. Introduction of a bulky benzyl ester group in 4 results in a shift in the pairwise O···H interaction from an aromatic proton to a methylene

proton and a concurrent lengthening in the interaction distance. Compound **4** is also the only compound in this series to display a pairwise O···H interaction involving *both* carbonyl functionalities. For compounds **2–4** the pyridyl nitrogen cannot participate in any intermolecular interactions due to the sterically bulky ester groups, but this is not the case for the smaller methyl ester **1**, which displays a completely different structure. Br···Br interactions also play a role in the structures, with close contacts observed for **2** and **4**. Both of these are type-I interactions, which minimize steric and electrostatic repulsion. However, while they result in a zigzag chain of Br atoms in **2**, **4** displays discrete pairs of Br···Br interactions.

The dipicolinic acid esters **2** and **4** were also extended *para* to the nitrogen, to give **5** and **6**, respectively, in which both contain a phenyl spacer. A complete loss of the pairwise O···H interaction was observed in **5**, with the dominant structure-directing motif now comprising  $\pi$ -based interactions. In **5** the pyridyl nitrogen and the ester oxygens do not participate in intermolecular interactions, as also seen in **2–4**. Instead of participating in a pairwise interaction, the carbonyl oxygens in **5** instead interact with ester protons in a manner similar to that observed in **3**. The introduction of a bulkier yet more flexible benzyl ester in compound **6** results in the return of the pairwise O···H interaction as observed in **1–3**, but this pairwise interaction is unique, distinguished by a third interaction between one carbonyl oxygen and a proton from the phenyl spacer. Hirshfeld surface analysis was employed for **1–6**, allowing quantification of these various interactions within the structures and identification of contacts that are not immediately apparent from individual crystal structures, such as the CH··· $\pi$  interactions observed in **5** and **6**. We have shown through systematic variation of dipicolinic acid derivatives, both at the ester positions and *para* to the pyridyl nitrogen, that we can achieve a degree of control over the behavior of these systems in the solid state and influence the dominant structure-directing features that are present.

## EXPERIMENTAL SECTION

**Synthesis of Compounds 1–4.** Chelidamic acid hydrate (500 mg, 2.74 mmol) was mixed with phosphorus pentabromide (5.0 g, 11.6 mmol) and heated to 90 °C until a viscous melt was produced. This melt was maintained at temperature for a further 1.5 h at which point it was cooled and CHCl<sub>3</sub> (10 mL) added. The resulting yellow precipitate was filtered and the appropriate alcohol (50 mL, methanol, ethanol, isopropanol, or benzyl alcohol for **1**, **2**, **3**, or **4**, respectively) added dropwise and the resulting solution stirred for 16 h. The solvent was removed under reduced pressure, water (50 mL) and ice (50 g) added, and the resulting precipitate filtered.

Diffraction data for **1–6** was collected using  $\omega$ -scans on an Agilent SuperNova CCD diffractometer equipped with a Cu-K $\alpha$  microfocus sealed tube X-ray source. Experimental temperatures were regulated using an Oxford Cryosystems open-flow nitrogen cryostat. Structures were solved by direct methods using SHELXS97<sup>32</sup> and refined against F<sup>2</sup> using SHELXL97.<sup>20</sup> Unless otherwise stated, all non-H atoms were refined with anisotropic atomic displacement parameters, while the hydrogen atoms were placed in geometrically calculated positions. Hirshfeld surface analysis was undertaken using CrystalExplorer 3.1.<sup>33</sup> For compound **3**, the disorder was modeled by running the Hirshfeld surface analysis for both possible orientations of the propyl esters. On the basis that the proportion of interactions varied by <0.4%, one orientation was selected and modeled as fully occupied.

**Crystal Data for 1.** C<sub>9</sub>H<sub>8</sub>BrNO<sub>4</sub>, M = 274.07, triclinic P $\bar{1}$  (No. 2),  $a$  = 3.9543(4),  $b$  = 13.6225(17),  $c$  = 18.749(2) Å,  $\alpha$  = 98.438(10),  $\beta$  = 93.014(9),  $\gamma$  = 97.680(9)°,  $V$  = 987.4(2) Å<sup>3</sup>,  $Z$  = 4,  $T$  = 120(2) K,

D<sub>calcd</sub> = 1.843 g cm<sup>-3</sup>,  $\mu$  = 5.673 mm<sup>-1</sup>, N(unique) = 3267 (merged from 6326), R<sub>int</sub> = 0.0301, R<sub>1</sub> = 0.0323, wR<sub>2</sub> (all data) = 0.0858, GOF = 1.03,  $\Delta\rho_{\max}$  = 0.54 e Å<sup>-3</sup>.

**Crystal Data for 2.** C<sub>11</sub>H<sub>12</sub>BrNO<sub>4</sub>, M = 302.13, monoclinic P2<sub>1</sub>/n (No. 14),  $a$  = 15.3907(6),  $b$  = 4.33847(15),  $c$  = 19.5380(8) Å,  $\beta$  = 110.046(4)°,  $V$  = 1225.56(8) Å<sup>3</sup>,  $Z$  = 4,  $T$  = 120(2) K, D<sub>calcd</sub> = 1.637 g cm<sup>-3</sup>,  $\mu$  = 4.630 mm<sup>-1</sup>, N(unique) = 2336 (merged from 14024), R<sub>int</sub> = 0.0248, R<sub>1</sub> = 0.0214, wR<sub>2</sub> (all data) = 0.0568, GOF = 1.05,  $\Delta\rho_{\max}$  = 0.31 e Å<sup>-3</sup>.

**Compound 3.** MP 90–91 °C; IR  $\nu_{\max}$  (cm<sup>-1</sup>): 3073, 2964, 2938, 2879, 1716, 1560, 1463, 1415, 1394, 1379, 1349, 1323, 1300, 1263, 1173, 1147, 978, 942, 925, 900, 793, 780, 760, 732, 690. <sup>1</sup>H NMR (270 MHz):  $\delta$  8.41 (s, 2H), 4.38 (t,  $J$  = 6.2 Hz, 4H), 1.85 (q,  $J$  = 7.5 Hz, 4H), 1.04 (t,  $J$  = 6.2 Hz, 6H). <sup>13</sup>C NMR (67.5 MHz):  $\delta_c$  163.6, 149.6, 135.0, 131.1, 68.2, 22.0, 10.4. HRMS (EI) m/z calcd for C<sub>13</sub>H<sub>17</sub>O<sub>4</sub>NBr: 330.043. Found for C<sub>13</sub>H<sub>17</sub>O<sub>4</sub>NBr: C, 47.3%; H, 4.9%; N, 4.2%; found C, 47.2%; H, 4.9%; N, 4.2%.

**Crystal Data for 3.** C<sub>13</sub>H<sub>16</sub>BrNO<sub>4</sub>, M = 330.18, monoclinic P2<sub>1</sub>/n (No. 14),  $a$  = 11.4027(4),  $b$  = 4.51826(15),  $c$  = 27.8897(11) Å,  $\beta$  = 99.456(4)°,  $V$  = 1417.36(9) Å<sup>3</sup>,  $Z$  = 4,  $T$  = 120(2) K, D<sub>calcd</sub> = 1.547 g cm<sup>-3</sup>,  $\mu$  = 4.055 mm<sup>-1</sup>, N(unique) = 2453 (merged from 8675), R<sub>int</sub> = 0.0308, R<sub>1</sub> = 0.0307, wR<sub>2</sub> (all data) = 0.0765, GOF = 1.05,  $\Delta\rho_{\max}$  = 0.45 e Å<sup>-3</sup>.

**Compound 4.** MP 87–88 °C; IR  $\nu_{\max}$  (cm<sup>-1</sup>): 3074, 2965, 2937, 2879, 2166, 1716, 1563, 1379, 1349, 1325, 1264, 1239, 1175, 1147, 944, 925, 900, 780, 700, 690. <sup>1</sup>H NMR (270 MHz):  $\delta$  8.42 (s, 2H), 7.51–7.46 (m, 4H), 7.43–7.34 (m, 6H), 5.46 (s, 4H). <sup>13</sup>C NMR (67.5 MHz):  $\delta_c$  163.6, 149.6, 135.0, 131.2, 128.8, 128.7, 128.6, 127.4, 68.1. HRMS (EI) m/z calcd C<sub>21</sub>H<sub>17</sub>NO<sub>4</sub>Br: 426.024. Found 426.032. Calcd for C<sub>21</sub>H<sub>17</sub>NO<sub>4</sub>Br: C, 59.2%; H, 3.8%; N, 3.3%; found C, 59.2%; H, 3.8%; N, 3.2%.

**Crystal Data for 4.** C<sub>21</sub>H<sub>16</sub>BrNO<sub>4</sub>, M = 426.26, triclinic P $\bar{1}$  (No. 2),  $a$  = 6.6580(4),  $b$  = 10.5799(11),  $c$  = 13.4275(4) Å,  $\alpha$  = 87.325(5),  $\beta$  = 81.672(4),  $\gamma$  = 75.385(7)°,  $V$  = 905.55(12) Å<sup>3</sup>,  $Z$  = 2,  $T$  = 120(2) K, D<sub>calcd</sub> = 1.563 g cm<sup>-3</sup>,  $\mu$  = 3.332 mm<sup>-1</sup>, N(unique) = 3071 (merged from 8212), R<sub>int</sub> = 0.0433, R<sub>1</sub> = 0.130, wR<sub>2</sub> (all data) = 0.393, GOF = 1.81,  $\Delta\rho_{\max}$  = 6.72 e Å<sup>-3</sup>.

**Synthesis of Compound 5.** Compound **2** (700 mg, 2.32 mmol), benzene-1,4-diboronic acid (175 mg, 1.06 mmol), and K<sub>2</sub>CO<sub>3</sub> (801 mg, 5.80 mmol) were suspended in toluene (100 mL) and water (25 mL). The solution was vigorously stirred and under Ar for 1 h at 60 °C. After this time [Pd<sub>2</sub>(dba)<sub>3</sub>] (214 mg, 0.23 mmol) and P('Bu)<sub>3</sub> (0.50 mL, 0.54 mmol) were added and the solution refluxed at 80 °C for 15 min. The solution was cooled, filtered through a silica plug using CH<sub>2</sub>Cl<sub>2</sub>, and the solvent removed under reduced pressure to afford **5** (534 mg, 97%) as a crystalline white powder.

**Compound 5.** MP 241–243 °C; IR  $\nu_{\max}$  (cm<sup>-1</sup>): 2984, 1716, 1601, 1558, 1474, 1402, 1374, 1344, 1323, 1266, 1242, 1149, 1111, 1074, 1026, 994, 941, 912, 883, 866, 844, 780, 752, 736, 729, 703, 555. <sup>1</sup>H NMR (270 MHz, DMSO-*d*<sub>6</sub>):  $\delta$  8.58 (s, 4H), 7.95 (s, 4H), 4.55 (q,  $J$  = 7.3 Hz, 8H), 1.51 (t,  $J$  = 7.4 Hz, 12H). <sup>13</sup>C NMR (67.5 MHz, DMSO-*d*<sub>6</sub>):  $\delta_c$  164.7, 149.7, 149.5, 137.9, 128.2, 125.5, 62.6, 14.3; HRMS (EI) m/z calcd for C<sub>28</sub>H<sub>28</sub>O<sub>8</sub>N<sub>2</sub>Na: 407.052; found 407.050. Calcd for C<sub>28</sub>H<sub>28</sub>O<sub>8</sub>N<sub>2</sub>·2.6CHCl<sub>3</sub>: C, 47.9%; H, 4.0%; N, 3.4%; found C, 48.0%; H, 4.0%; N, 3.8%.

**Crystal Data for 5.** C<sub>28</sub>H<sub>28</sub>N<sub>2</sub>O<sub>8</sub>, M = 520.52, triclinic P $\bar{1}$  (No. 2),  $a$  = 6.7914(5),  $b$  = 10.0137(7),  $c$  = 10.9532(10) Å,  $\alpha$  = 113.673(7),  $\beta$  = 92.345(6),  $\gamma$  = 107.500(6)°,  $V$  = 639.4(1) Å<sup>3</sup>,  $Z$  = 1,  $T$  = 120(2) K, D<sub>calcd</sub> = 1.352 g cm<sup>-3</sup>,  $\mu$  = 0.831 mm<sup>-1</sup>, N(unique) = 2253 (merged from 4245), R<sub>int</sub> = 0.0158, R<sub>1</sub> = 0.0352, wR<sub>2</sub> (all data) = 0.0966, GOF = 1.06,  $\Delta\rho_{\max}$  = 0.22 e Å<sup>-3</sup>.

**Synthesis of Compound 6.** Compound **4** (100 mg, 0.235 mmol), benzene-1,4-diboronic acid (18 mg, 0.107 mmol), and K<sub>2</sub>CO<sub>3</sub> (81 mg, 0.59 mmol) were suspended in toluene (20 mL) and water (5 mL). The solution was vigorously stirred under Ar for 1 h at 60 °C. After this time [Pd<sub>2</sub>(dba)<sub>3</sub>] (22 mg, 0.023 mmol) and P('Bu)<sub>3</sub> (50  $\mu$ L, 0.056 mmol) were added and the solution refluxed at 80 °C for 15 min. The solution was cooled, filtered through a silica plug using CH<sub>2</sub>Cl<sub>2</sub>, and the solvent removed under reduced pressure to afford **6** (60 mg, 73%) as a white powder.

**Compound 6.** MP 263–265 °C; IR  $\nu_{\text{max}}$ (cm<sup>-1</sup>): 3071, 2965, 2940, 2884, 2145, 1718, 1560, 1375, 1344, 1328, 1264, 1240, 1148, 943, 895, 780, 705. <sup>1</sup>H NMR (270 MHz): δ<sub>c</sub> 8.53 (s, 4H), 7.88 (s, 4H), 7.54–7.50 (m, 4H), 7.43–7.34 (m, 6H), 5.51 (s, 4H). <sup>13</sup>C NMR (67.5 MHz): δ<sub>c</sub> 163.9, 152.3, 149.7, 149.4, 137.9, 129.4, 128.8, 125.8, 125.6, 121.8. HRMS (EI) *m/z* calcd for C<sub>28</sub>H<sub>28</sub>O<sub>8</sub>N<sub>2</sub>Na: 769.255; found 769.248.

**Crystal Data for 6.** C<sub>48</sub>H<sub>36</sub>N<sub>2</sub>O<sub>8</sub>, M = 768.83, triclinic P $\overline{1}$  (No. 2),  $a$  = 9.6784(6),  $b$  = 10.0930(8),  $c$  = 19.0710(19) Å,  $\alpha$  = 88.546(7),  $\beta$  = 85.079(7),  $\gamma$  = 82.955(6)°, V = 1841.8(3) Å<sup>3</sup>, Z = 2, T = 120(2) K, D<sub>calcd</sub> = 1.386 g cm<sup>-3</sup>,  $\mu$  = 0.773 mm<sup>-1</sup>, N(unique) = 7178 (merged from 11316), R<sub>int</sub> = 0.0750, R<sub>1</sub> = 0.0604, wR<sub>2</sub> (all data) = 0.1401, GOF = 1.01, Δρ<sub>max</sub> = 0.46 e Å<sup>-3</sup>.

## ■ ASSOCIATED CONTENT

### Supporting Information

CIF files for compounds 1 – 6. This material is available free of charge via the Internet at <http://pubs.acs.org>.

## ■ AUTHOR INFORMATION

### Corresponding Author

\*E-mail: m.schroder@nottingham.ac.uk.

### Notes

The authors declare no competing financial interest.

## ■ ACKNOWLEDGMENTS

We thank the EPSRC and University of Nottingham for support. M.S. acknowledges receipt of an ERC Advanced Grant.

## ■ REFERENCES

- Desiraju, G. R.; Vittal, J. J.; Ramanan, A. *Crystal Engineering: A Textbook*; World Scientific Publishing: Singapore, 2011.
- Schmidt, A.; Casini, A.; Kuhn, F. E. *Coord. Chem. Rev.* **2014**, *275*, 19–36.
- Hu, X. Y.; Xiao, T. X.; Lin, C.; Huang, F. H.; Wang, L. Y. *Acc. Chem. Res.* **2014**, *47*, 2041–2051.
- Tanaka, S.; Tsurugi, H.; Mashima, K. *Coord. Chem. Rev.* **2014**, *65*, 38–51.
- Busseron, E.; Ruff, Y.; Moulin, E.; Giuseppone, N. *Nanoscale* **2013**, *5*, 7098–7140.
- Lindoy, L. F.; Park, K. M.; Lee, S. S. *Chem. Soc. Rev.* **2013**, *14*, 1713–1727.
- Burrows, A. D. *Struct. Bonding* **2004**, *108*, 55–96.
- Baruah, P. K.; Khan, S. *RSC Adv.* **2013**, *3*, 21202–21217.
- Mali, K. S.; Adisoejoso, J.; Ghijssens, E.; De Cat, I.; De Feyter, S. *Acc. Chem. Res.* **2012**, *45*, 1309–1320.
- Rybchinski, B. *ACS Nano* **2011**, *5*, 6791–6818.
- Friščić, T. *Chem. Soc. Rev.* **2012**, *41*, 3493–3510.
- Spackman, M. A.; Jayatilaka, D. *CrystEngComm* **2009**, *11*, 19–32.
- McKinnon, J. J.; Spackman, M. A.; Mitchell, A. S. *Acta Crystallogr., Sect. B* **2004**, *B60*, 627–668.
- Munshi, P.; Jelsch, C.; Hathwar, V. R.; Guru Row, T. N. *Cryst. Growth Des.* **2010**, *10*, 1516–1526.
- Ling, I.; Alias, Y.; Sobolev, A. N.; Raston, C. L. *New J. Chem.* **2010**, *34*, 414–419.
- Martin, A. D.; Hartlieb, K. J.; Sobolev, A. N.; Raston, C. L. *Cryst. Growth Des.* **2010**, *10*, 5302–5306.
- Lessmann, J. J.; Horrocks, W. D., Jr. *Inorg. Chem.* **2000**, *39*, 3114–3124.
- Prasad, T. K.; Sailaja, S.; Rajasekharan, M. V. *Polyhedron* **2005**, *24*, 1487–1496.
- Latva, M.; Takalo, H.; Simberg, K.; Kankare, J. *J. Chem. Soc., Perkin Trans. 2* **1995**, 995–999.
- Kirillova, M. V.; Kirillov, A. M.; da Silva, M. F. C. G.; Pombeiro, A. J. L. *Eur. J. Inorg. Chem.* **2008**, *22*, 3423–3427.
- Felloni, M.; Blake, A. J.; Hubberstey, P.; Wilson, C.; Schröder, M. *Crystal Growth Des.* **2009**, *9*, 4685–4699.
- Felloni, M.; Blake, A. J.; Hubberstey, P.; Teat, S. J.; Wilson, C.; Schröder, M. *CrystEngComm* **2010**, *12*, 1576–1589.
- Lin, X.; Blake, A. J.; Wilson, C.; Sun, X. Z.; Champness, N. R.; George, M. W.; Hubberstey, P.; Mokaya, R.; Schröder, M. *J. Am. Chem. Soc.* **2006**, *128*, 10745–10753.
- Kirin, S. I.; Ohr, K.; Yennawar, H. P.; Morgan, C. M.; Levine, L. A.; Williams, M. E. *Inorg. Chem.* **2007**, *10*, 652–656.
- Liu, Y.-R.; Yang, T.; Li, L.; Liu, J.-M.; Su, C.-Y. *Aust. J. Chem.* **2009**, *62*, 1667–1674.
- Prior, K. E.; Shipps, G. W., Jr.; Skyler, D. A.; Rebek, J., Jr. *Tetrahedron* **1998**, *54*, 4107–4124.
- Moreau, F.; Audebrand, N.; Poriel, C.; Moizan-Basle, V.; Ouvry, J. *J. Mater. Chem.* **2011**, *21*, 18715–1722.
- McKinnon, J. J.; Jayatilaka, D.; Spackman, M. A. *Chem. Commun.* **2007**, 3814–3816.
- Brezgunova, M. E.; Aubert, E.; Dahaoui, S.; Fertey, P.; Lebegue, S.; Jelsch, C.; Anyan, J. G.; Espinosa, E. *Cryst. Growth Des.* **2012**, *12*, 5373–5376.
- Desiraju, G. R.; Parthasarathy, R. *J. Am. Chem. Soc.* **1989**, *111*, 8725–8726.
- Pedireddi, V. R.; Reddy, D. S.; Goud, B. S.; Rae, D. C.; Desiraju, G. R. *J. Chem. Soc., Perkin Trans. 2* **1994**, 2353–2360.
- Sheldrick, G. M. *Acta Crystalogr., Sect. A* **2008**, *64*, 112–122.
- Wolff, S. K.; Grimwood, D. J.; McKinnon, J. J.; Turner, M. J.; Jayatilaka, D.; Spackman, M. A. *CrystExplor* 3.1; University of Western Australia: Crawley, Australia, 2012.